processes

MDPI

Article

Shear Rate Coat-Hanger Die Using Casson Viscosity Model

Dastan Igali [1], Asma Perveen [1], Dichuan Zhang [2] and Dongming Wei [3,*]

[1] Department of Mechanical and Aerospace Engineering, School of Engineering and Digital Sciences, Nazarbayev University, Nur-Sultan City 010000, Kazakhstan; dastan.igali@nu.edu.kz (D.I.); asma.perveen@nu.edu.kz (A.P.)

[2] Department of Civil and Environmental Engineering, School of Engineering and Digital Sciences, Nazarbayev University, Nur-Sultan City 010000, Kazakhstan; dichuan.zhang@nu.edu.kz

[3] Department of Mathematics, School of Sciences and Humanities, Nazarbayev University, Nur-Sultan City 010000, Kazakhstan

* Correspondence: dongming.wei@nu.edu.kz; Tel.: +7-71-7270-9388

Received: 20 August 2020; Accepted: 14 October 2020; Published: 24 November 2020

Abstract: Coat-hanger die design aims for optimization of the die geometry of the body and the flow distribution manifold, such that through the exit at the die lip homogeneous distribution of the polymer melt is achieved. This paper proposes a novel methodology for deriving the design equations of the coat-hanger die geometry for some specific extrusion materials and provides fluid–solid interaction simulations for validations. The basis for the calculations is the Casson rheological model, analytic velocity profiles for the pseudoplastic flow through circular pipe and slit, and the constant shear rate coat-hanger die design methodology developed by Winter and Fritz. The geometry obtained was then evaluated using the fluid-structure interaction numerical simulation approach. The sensitivity of the outlet velocity uniformity and die body deformation due to the material and mass flow rate change were investigated using the finite element software, Ansys. It was found that the homogeneity of the outlet velocity is very sensitive to the extrusion materials. The structural analysis of the solid die body also resulted in higher deformations when using some other extrusion materials different from the initial design. Mass flow rate increase only resulted in large zones of stagnation, which occurred around the melt as it passes from the manifold to the slit region. Therefore, it is recommended to define the required range of mass flow rate to prevent the formation of stagnation zones.

Keywords: polymer extrusion; coat-hanger dies; uniform wall shear rate; power-law; Casson model

1. Introduction

The coat-hanger extrusion die design is mainly focused on the geometry optimization of the flow channels capable of providing homogenous distribution of the polymer melt across the die width [1–3]. There are a number of studies assessing the velocity uniformity of the polymer melt at the exit by means of the computational fluid dynamics (CFD) approach [4–9]. Few studies carried out the fluid-structure interaction (FSI) method to evaluate the velocity distribution of the coat-hanger die with the manifold of the rectangular cross-section when the solid die body is subject to deflection [10].

The mostly used and adequate mathematical design method focusing on the distribution problem was proposed by Winter and Fritz [11] in 1986. Winter and Fritz [11] claimed that their design method is practically independent of flow rate and viscosity of the polymer melt being extruded. The proposed design approach is based on a flow model assuming power-law viscosity and uniform shear rate at the walls of the manifold and slit regions [11].

There are multiple viscosity models used by the thin film/sheets industries and scientists to describe the non-Newtonian flow behavior of the polymer melts, including power-law, Cross law,

Carreau–Yasuda law, and Herschel–Bulkley model. The power-law is known as the most preferable and accurate viscosity model despite its simplicity [5]. Aforementioned laws except for the power-law model have never been used for deriving the design equations of the coat-hanger die because of their complexity.

The rheological model known as the Casson model [12] is mainly applied to describe the non-Newtonian flow behavior of blood and chocolate [13–15]. There are some studies [16,17] that mentioned the application of the Casson model in polymer industries, and few studies [18,19] considered the Casson model for the rheological analysis of the polymer melts. According to Lungu et al. [18], there is a good agreement between the Casson model based theoretical flow curves and experimental data. In addition, Matveenko and Kirsanov [19] claimed that the coefficients of the generalized Casson rheological model better describes the pseudoplastic behavior of the polymer melts compared to the commonly used power-law model in some application conditions.

This paper aims to develop the procedure of deriving the design equations for the uniform shear rate coat-hanger die based on the Casson viscosity model as an alternative to the design method proposed by Winter and Fritz [11]. The fundamental equations used in this mathematical modeling are taken from the studies of Hopmann and Michaeli [20] and Winter and Fritz [11]. In addition, the performance of the model created is evaluated using the fluid-structure interaction (FSI) approach in the engineering simulation software Ansys Workbench 15.9. Thereafter, the sensitivity of the outlet velocity to the design parameters, such as operating mass flow rates and rheological behavior of the materials, is discussed. The deformation of the solid die body due to high internal pressures within the viscous polymer melt is also studied.

2. Mathematical Modeling

2.1. General

In this section, the design equations for the uniform shear rate coat-hanger die with circular manifold and slit region of rectangular cross-section are derived. The uniform wall shear rate dies can provide uniform distribution of the melt across the die exit, which is invariant to the changes in polymer melt viscosity [11] for power-law flows. The basis for the calculations that pertain to the polymer flow processes are mass, momentum, and energy conservation laws, Casson rheological model [12], and the design methodology used by Winter and Fritz [11] for the power-law viscosity model.

To demonstrate the design procedure, the simple schematics of the coat-hanger distribution system with a circular manifold of varying radius and narrow slit flow region, shown in Figure 1, is used. We are given the height of the slit flow region $H = 0.003$ m, half width of the die lip $B = 0.360$ m, and the volumetric flow rate for the die $\dot{V} = 10^{-3} \frac{m^3}{s}$.

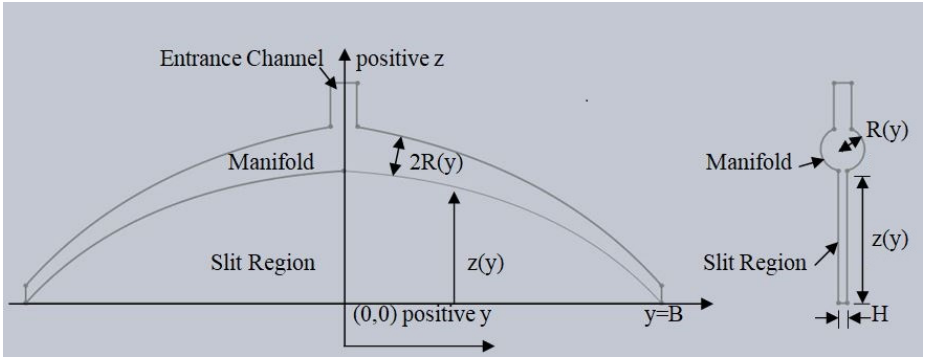

Figure 1. Front view, central cross-section.

According to Figure 1, the flow rate in the manifold region decreases with decreasing manifold radius R(y) in positive y direction. The simple mass balance Equation is applied implying that the

flow rate of the material passing through the manifold channel $Q_m(y)$ is equal to the flow rate of the material coming out of the die exit between y and B, $Q_s(y)$.

$$Q_m(y) = Q_s(y), \tag{1}$$

$$\pi R^2(y) v_m = (B - y) \cdot H v_s, \tag{2}$$

For the momentum balance, it is assumed that the melt transition from the circular manifold into the rectangular slit region does not significantly affect the pressure gradient in the manifold. The pressure gradients in both the manifold and slit regions that are normal to their corresponding cross-sections are constant throughout the cross-sections. The relationship between the pressure gradients can be represented as follows:

$$\left(\frac{dp}{dz}\right)_s = \left(\frac{dp}{d\xi}\right)_m \cdot \frac{\Delta\xi}{\Delta z}, \tag{3}$$

where $\Delta\xi$, is the small length element in the flow direction through the manifold and Δz is the length element in the flow direction through the slit (z-direction). Furthermore, we have the following relationship between $\Delta\xi$, and Δz:

$$\Delta\xi = \Delta z \cdot \sqrt{1 + \left(\frac{dz}{dy}\right)^{-2}}, \tag{4}$$

where $\frac{dz}{dy}$ is the slope of the contour line $z(y)$ representing the curvature of the manifold. The combination of Equations (3) and (4) [11] gives the following result:

$$\frac{dz}{dy} = -\left[\left(\frac{(dp/dz)_s}{(dp/d\xi)_m}\right)^2 - 1\right]^{-\frac{1}{2}}, \tag{5}$$

There are also some basic assumptions that were made for the computations:

- Steady state flow;
- Isothermal flow;
- Hydrodynamically fully developed flow;
- Incompressible fluid;
- No external forces (e.g., the effect of gravity is neglected);
- No slip boundary condition;
- Uniform shear rate at the walls of the manifold and slit region.
-] The radius of the manifold at the edge $R(y = 0.36\ \text{m})$ is equal to the half-height of the slit $H = 0.0015$ m.

2.2. Casson Model-Based Design Equations

It is essential to introduce the Casson model as it is used to describe the non-Newtonian flow behavior of the polymer melt. The mathematical form of Casson model is given by:

$$\sqrt{\tau} = \sqrt{\tau_0} + \sqrt{k} \cdot \sqrt{\dot{\gamma}}, \tag{6}$$

where τ is the shear stress, τ_0 is the yield stress, k is the viscosity coefficient for Casson fluid, and $\dot{\gamma}$ is the shear rate. The polymer material for which the coat-hanger die design example is developed has the following properties; for the design example, the parameters values $\tau_0 = 1.062$ Pa and $k = 0.0271$ Pa s are adopted from [21].

Equations (2), (5), and (6) are the basics for deriving the flow distribution manifold design equations.

From Equation (6) it follows that

$$\dot{\gamma} = \left(\frac{\sqrt{\tau} - \sqrt{\tau_0}}{\sqrt{k}} \right)^2, \tag{7}$$

To satisfy the uniform wall shear rate condition, we should have

$$\dot{\gamma}_{w,s} = \dot{\gamma}_{w,m}, \tag{8}$$

which also means the following:

$$\left(\frac{\sqrt{\tau_{w,s}} - \sqrt{\tau_0}}{\sqrt{k}} \right)^2 = \left(\frac{\sqrt{\tau_{w,m}} - \sqrt{\tau_0}}{\sqrt{k}} \right)^2 \tag{9}$$

which in turn leads to the following:

$$\tau_{w,s} = \tau_{w,m}, \tag{10}$$

The wall shear stresses for the manifold and slit regions satisfying the condition in Equation (10) will be separately examined in Sections 2.2.1 and 2.2.2.

2.2.1. Manifold Region

According to Hopmann and Michaeli [20], the shear stress Equation for the circular pipe is:

$$\tau = \frac{\Delta p \cdot r}{2 \cdot L_\xi}, \tag{11}$$

The shear stress at the walls of the circular pipe of the radius R is calculated as:

$$\tau_w = \tau(r = R) = \frac{\Delta p \cdot R}{2 \cdot L_\xi}, \tag{12}$$

By substituting $a = \frac{\Delta p}{2 \cdot L_\xi}$ into Equation (11) we obtain:

$$\tau = a \cdot r, \tag{13}$$

Hence, Equation (7) can be rewritten as:

$$\dot{\gamma} = \left(\frac{\sqrt{a \cdot r} - \sqrt{\tau_0}}{\sqrt{k}} \right)^2, \tag{14}$$

It is also known that:

$$\dot{\gamma} = -\frac{dv_z(r)}{dr}, \tag{15}$$

Combining the Equations (14) and (15), we obtain:

$$-\frac{dv_z(r)}{dr} = \left(\frac{\sqrt{a \cdot r} - \sqrt{\tau_0}}{\sqrt{k}} \right)^2, \tag{16}$$

From above:

$$dv_z(r) = -\left(\frac{\sqrt{a \cdot r} - \sqrt{\tau_0}}{\sqrt{k}} \right)^2 \cdot dr, \tag{17}$$

After integration and considering the boundary condition $v_z(r = R) = 0$ (no slip boundary condition), the velocity distribution over the cross-section of the circular pipe follows:

$$v_z(r) = \frac{1}{k} \left[\frac{4}{3} \sqrt{a\tau_0} \left(r^{\frac{3}{2}} - R^{\frac{3}{2}} \right) + \frac{a}{2} \left(R^2 - r^2 \right) + \tau_0 (R - r) \right], \tag{18}$$

For the mean velocity $\overline{v}_z$:

$$\overline{v}_z = \frac{1}{A}\int_0^R v_z(r)dA \text{ with } A = \pi \cdot R^2 \text{ and } dA = 2 \cdot \pi \cdot r \cdot dr, \tag{19}$$

From the above we obtain:

$$\overline{v}_z = \frac{2}{kR^2}\left[-\frac{2}{7}\sqrt{a\tau_0}R^{\frac{7}{2}} + a\frac{R^4}{8} + \tau_0\frac{R^3}{6}\right], \tag{20}$$

After solving the Equation (20) using Maple Software (Release 2020.0) for $a = \frac{\Delta p}{2 \cdot L}$, we obtain the following two roots:

$$a_1 = -\frac{4}{21}\frac{7R^{\frac{3}{2}}\tau_0 - 21\sqrt{R}k\overline{v}_z - \frac{8}{7}\cdot\frac{12R^{\frac{7}{2}}\tau_0 + \sqrt{-3R^7\tau_0{}^2 + 441R^6k\overline{v}_z\tau_0}}{R^2}}{R^{\frac{5}{2}}}, \tag{21}$$

$$a_2 = -\frac{4}{21}\frac{7R^{\frac{3}{2}}\tau_0 - 21\sqrt{R}k\overline{v}_z - \frac{8}{7}\cdot\frac{12R^{\frac{7}{2}}\tau_0 - \sqrt{-3R^7\tau_0{}^2 + 441R^6k\overline{v}_z\tau_0}}{R^2}}{R^{\frac{5}{2}}}, \tag{22}$$

When substituting the first root for a into Equation (23):

$$\tau = -\frac{4}{21}\frac{7R^{\frac{3}{2}}\tau_0 - 21\sqrt{R}k\overline{v}_z - \frac{8}{7}\cdot\frac{12R^{\frac{7}{2}}\tau_0 + \sqrt{-3R^7\tau_0{}^2 + 441R^6k\overline{v}_z\tau_0}}{R^2}}{R^{\frac{5}{2}}} \cdot r, \tag{23}$$

For the shear stress at the wall, $\tau_w(r = R)$:

$$\tau_w = -\frac{4}{21}\frac{7R^{\frac{3}{2}}\tau_0 - 21\sqrt{R}k\overline{v}_z - \frac{8}{7}\cdot\frac{12R^{\frac{7}{2}}\tau_0 + \sqrt{-3R^7\tau_0{}^2 + 441R^6k\overline{v}_z\tau_0}}{R^2}}{R^{\frac{3}{2}}}, \tag{24}$$

As this Equation is valid for the manifold region, $\overline{v}_z$ was replaced by $\overline{v}_{z,m}$:

$$\tau_{w,m} = -\frac{4}{21}\frac{7R^{\frac{3}{2}}\tau_0 - 21\sqrt{R}k\overline{v}_{z,m} - \frac{8}{7}\cdot\frac{12R^{\frac{7}{2}}\tau_0 + \sqrt{-3R^7\tau_0{}^2 + 441R^6k\overline{v}_{z,m}\tau_0}}{R^2}}{R^{\frac{3}{2}}}, \tag{25}$$

The volumetric flow rate $\dot{V}$ is obtained using the following:

$$\dot{V} = \overline{v}_z \cdot A \text{ where } A = \pi \cdot R^2, \tag{26}$$

Combining Equations (20) and (26), we obtain:

$$\dot{V} = \frac{2\pi}{k}\left[-\frac{2}{7}\sqrt{a\tau_0}R^{\frac{7}{2}} + a\frac{R^4}{8} + \tau_0\frac{R^3}{6}\right], \tag{27}$$

Equation (27) will further be used in the evaluation of the design equations.

2.2.2. Slit Region

According to Hopmann and Michaeli [20], for the flow between two parallel plates, the shear stress is analogous to Equation (11):

$$\tau(x) = \frac{\Delta p}{L_z} \cdot x, \tag{28}$$

For the shear stress at the wall we have:

$$\tau_w = \tau\left(x = \frac{H}{2}\right) = \frac{\Delta p \cdot H}{2 \cdot L_z}, \tag{29}$$

substituting $b = \frac{\Delta p}{L_z}$ into Equation (28), we obtain:

$$\tau(x) = b \cdot x, \tag{30}$$

Thus, for the two parallel plates, Equation (7) can be rewritten as:

$$\dot{\gamma} = \left(\frac{\sqrt{b \cdot x} - \sqrt{\tau_0}}{\sqrt{k}}\right)^2, \tag{31}$$

In addition, noting that $\dot{\gamma} = -\frac{dv_z(r)}{dr}$ we have:

$$-\frac{dv_z(r)}{dr} = \left(\frac{\sqrt{b \cdot x} - \sqrt{\tau_0}}{\sqrt{k}}\right)^2, \tag{32}$$

Integrating over x and considering boundary condition $v_z\left(x = \frac{H}{2}\right) = 0$

$$v_z = \frac{1}{k}\left[\frac{4}{3}\sqrt{b \cdot \tau_0}\left(x^{\frac{3}{2}} - \left(\frac{H}{2}\right)^2\right) + \frac{b}{2}\left(\left(\frac{H}{2}\right)^2 - x^2\right) + \tau_0\left(\frac{H}{2} - x\right)\right], \tag{33}$$

Mean velocity:

$$\overline{v}_z = \frac{2}{H}\int_0^{\frac{H}{2}} v_z(x)dx = \frac{1}{k}\left[-\frac{4}{5}\sqrt{b\tau_0\left(\frac{H}{2}\right)^{\frac{3}{2}}} + \frac{1}{3}b\left(\frac{H}{2}\right)^2 + \frac{\tau_0}{2}\left(\frac{H}{2}\right)\right], \tag{34}$$

Using Maple Software to solve for b, the following roots of the above Equation were obtained:

$$b_1 = \frac{12}{25} \cdot \frac{\sqrt{2}\left(6\sqrt{2}H^{\frac{3}{2}}\tau_0 + \sqrt{-3H^3\tau_0{}^2 + 300H^2k\overline{v}_z\tau_0}\right) - 5H^{\frac{3}{2}}\tau_0 + 20\sqrt{H}k\overline{v}_z}{H^{\frac{5}{2}}}, \tag{35}$$

$$b_2 = \frac{12}{25} \cdot \frac{\sqrt{2}\left(6\sqrt{2}H^{\frac{3}{2}}\tau_0 - \sqrt{-3H^3\tau_0{}^2 + 300H^2k\overline{v}_z\tau_0}\right) - 5H^{\frac{3}{2}}\tau_0 + 20\sqrt{H}k\overline{v}_z}{H^{\frac{5}{2}}}, \tag{36}$$

Thus, substituting b_1 into Equation (30) we have:

$$\tau(x) = \frac{12}{25} \cdot \frac{\sqrt{2}\left(6\sqrt{2}H^{\frac{3}{2}}\tau_0 + \sqrt{-3H^3\tau_0{}^2 + 300H^2k\overline{v}_z\tau_0}\right) - 5H^{\frac{3}{2}}\tau_0 + 20\sqrt{H}k\overline{v}_z}{H^{\frac{5}{2}}} \cdot x, \tag{37}$$

The shear rate at the wall $\tau_w\left(x = \frac{H}{2}\right)$ is:

$$\tau_w = \frac{6}{25} \cdot \frac{\sqrt{2}\left(6\sqrt{2}H^{\frac{3}{2}}\tau_0 + \sqrt{-3H^3\tau_0{}^2 + 300H^2k\overline{v}_z\tau_0}\right) - 5H^{\frac{3}{2}}\tau_0 + 20\sqrt{H}k\overline{v}_z}{H^{\frac{3}{2}}}, \tag{38}$$

Then, replacing $\overline{v}_z$ by $\overline{v}_{z,s}$

$$\tau_{w,s} = \frac{6}{25} \cdot \frac{\sqrt{2}\left(6\sqrt{2}H^{\frac{3}{2}}\tau_0 + \sqrt{-3H^3\tau_0{}^2 + 300H^2k\overline{v}_{z,s}\tau_0}\right) - 5H^{\frac{3}{2}}\tau_0 + 20\sqrt{H}k\overline{v}_{z,s}}{H^{\frac{3}{2}}}, \tag{39}$$

The volumetric flow rate is evaluated by integrating over the cross-section:

$$\dot{V} = \int_{-\frac{H}{2}}^{\frac{H}{2}} \int_{0}^{B} v_z(x)dydx = \frac{BH}{k}\left[-\frac{4}{5}\sqrt{b\tau_0}\left(\frac{H}{2}\right)^{\frac{3}{2}} + \frac{1}{3}b\left(\frac{H}{2}\right)^2 + \frac{\tau_0}{2}\left(\frac{H}{2}\right)\right], \tag{40}$$

2.2.3. Computation of the Design Equations

In order to obtain the design equations for the uniform shear rate coat-hanger die, Equations (25) and (39) must satisfy the condition in Equation (10):

$$\begin{aligned} &-\frac{4}{21}\frac{7R^{\frac{3}{2}}\tau_0 - 21\sqrt{R}k\bar{v}_{z,m} - \frac{8}{7}\cdot\frac{12R^{\frac{7}{2}}\tau_0 + \sqrt{-3R^7\tau_0{}^2 + 441R^6k\bar{v}_{z,m}\tau_0}}{R^2}}{R^{\frac{3}{2}}} \\ &= \frac{6}{25}\cdot\frac{\sqrt{2}\left(6\sqrt{2}H^{\frac{3}{2}}\tau_0 + \sqrt{-3H^3\tau_0{}^2 + 300H^2k\bar{v}_{z,s}\tau_0}\right) - 5H^{\frac{3}{2}}\tau_0 + 20\sqrt{H}k\bar{v}_{z,s}}{H^{\frac{3}{2}}}, \end{aligned} \tag{41}$$

From this equation, we can calculate the mean velocity in the slit region using Maple Software. To simplify the calculation, all constants, including material characteristics τ_0 and k and size parameters B and H, are substituted:

$$\begin{aligned} v_{m,1} = \Big[&0.003429948352\sqrt{2.398350\cdot10^9 v_s - 2.819610\cdot10^6} + 500v_s + 26.58265683 + 1.265155509\cdot10^{-9} \\ &\sqrt{1.598900\cdot10^{22}v_s + 4.323402003\cdot10^{20} + 1.096828884\cdot10^{17}\sqrt{2.398350\cdot10^9 v_s - 2.819610\cdot10^6}}\Big]R, \end{aligned} \tag{42}$$

$$\begin{aligned} v_{m,2} = \Big[&0.003429948352\sqrt{2.398350\cdot10^9 v_s - 2.819610\cdot10^6} + 500v_s + 26.58265683 - 1.265155509\cdot10^{-9} \\ &\sqrt{1.598900\cdot10^{22}v_s + 4.323402003\cdot10^{20} + 1.096828884\cdot10^{17}\sqrt{2.398350\cdot10^9 v_s - 2.819610\cdot10^6}}\Big]R, \end{aligned} \tag{43}$$

Furthermore, the volumetric flow rate of the system can be written as:

$$\dot{V} = 2BH\bar{v}_s, \tag{44}$$

Rearranging the above, we obtain $\bar{v}_s$:

$$\bar{v}_s = \frac{\dot{V}}{2BH}, \tag{45}$$

Substituting the first root $v_{m,1}$ from Equation (42), Equation (45), and all constants in Equation (2), and then solving for $R(y)$ using Wolfram Mathematica, we obtain the first design Equation for the uniform shear rate coat-hanger die:

$$R(y) = \left(1.084\cdot10^{-6}\cdot(0.36 - x)\right)^{\frac{1}{3}}, \tag{46}$$

However, this Equation does not satisfy the condition concerning the manifold radius at $y = 0.36$ m, which must be equal to $R(y = 0.36\ m) = 0.0015$ m. Hence, we add 0.0015 m to Equation (46):

$$R(y) = \left(1.084\cdot10^{-6}\cdot(0.36 - x)\right)^{\frac{1}{3}} + 0.0015, \tag{47}$$

Combining Equations (6), (12), and (29), the following relations are obtained for the manifold and slit regions:

$$\frac{\Delta p\cdot R}{2\cdot L_\xi} = \left(\sqrt{\tau_0} + \sqrt{k}\sqrt{\dot{\gamma}_w}\right)^2, \tag{48}$$

$$\frac{\Delta p\cdot H}{2\cdot L_z} = \left(\sqrt{\tau_0} + \sqrt{k}\sqrt{\dot{\gamma}_w}\right)^2, \tag{49}$$

Rearranging the equations above:

$$\frac{dp}{d\xi} = \frac{2\left(\sqrt{\tau_0} + \sqrt{k}\sqrt{\dot{\gamma}_w}\right)^2}{R(y)}, \tag{50}$$

$$\frac{dp}{dz} = \frac{2\left(\sqrt{\tau_0} + \sqrt{k}\sqrt{\dot{\gamma}_w}\right)^2}{H}, \tag{51}$$

Substituting Equations (50) and (51) into Equation (10):

$$\frac{dz}{dy} = -\left[\left(\frac{R(y)}{H}\right)^2 - 1\right]^{-\frac{1}{2}}, \tag{52}$$

Substituting Equation (47) and $H = 0.0015$ m into Equation (52) and integrating over y in Wolfram Mathematica, we obtain $z(y)$:

$$z(y) = 1.1201{\cdot}10^6\left(3.21401{\cdot}10^{-7} - 8.9278{\cdot}10^{-7}y\right){}_2F_1 \left[0.5,\ 1.5,\ 2.5,\ -111111.\left(3.21401{\cdot}10^{-7} - 8.9278{\cdot}10^{-7}y\right)^{\frac{2}{3}}\right], \tag{53}$$

Equations (47) and (53) are called the design equations for the Casson model-based uniform shear rate coat-hanger die with circular cross-section manifold. The following geometry was created using these design equations as can be seen in Figure 2.

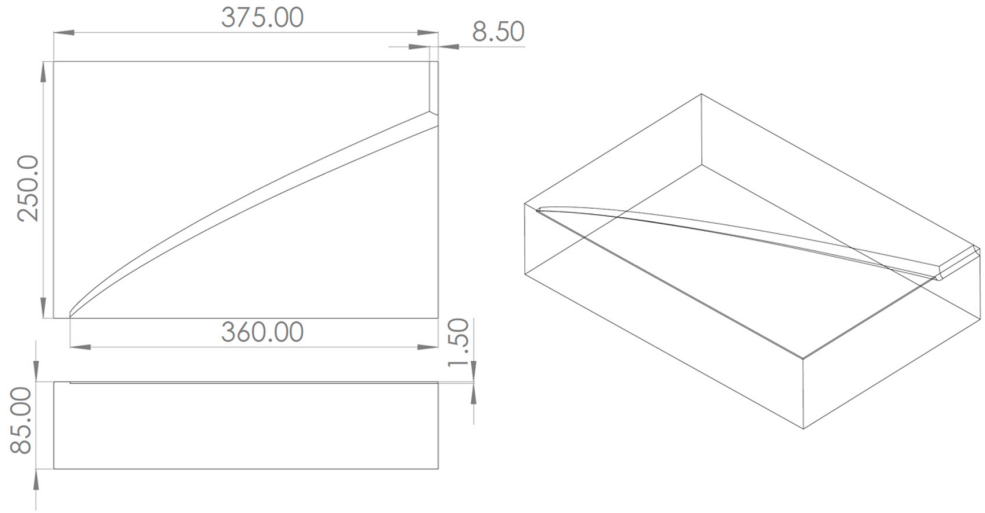

Figure 2. Casson model-based coat-hanger die geometry.

3. Computational Model

The FSI analysis of the polymer flow through the coat-hanger die will consider the following two domains: solid die body and polymer melt (Figure 3). The die body is assumed to be constructed of tool steel with a Young's modulus $E = 2.09{\cdot}10^{11}$ Pa, Poisson's ratio $\nu = 0.29$, and yield strength $\sigma_y = 1.03{\cdot}10^9$ Pa. Due to symmetric feature of the coat-hanger die geometry, only a quarter of the die body will be used in computation.

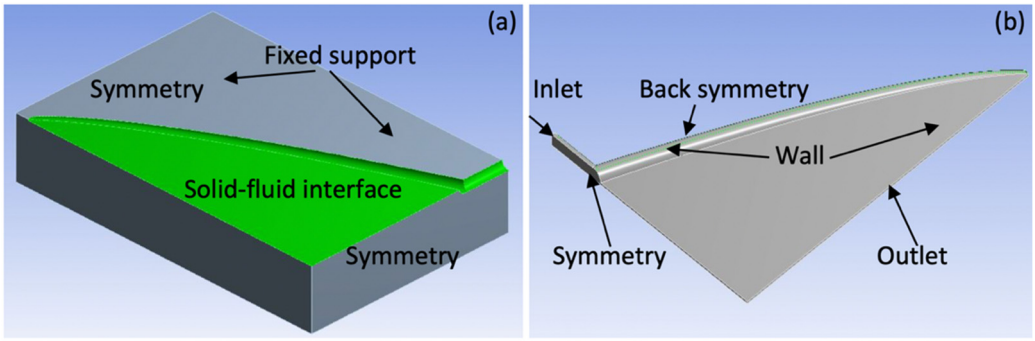

Figure 3. (**a**) Solid domain and (**b**) fluid domain.

The quantitative parameters of the coat-hanger die are summarized in Table 1. The geometry obtained for the coat-hanger is capable of providing a product of 720 mm width and 3 mm thickness.

Table 1. The quantitative parameters of the coat-hanger die.

Entrance Diameter, mm	Distance between Inlet and Outlet, mm	Thickness, mm	Width, mm	Height of the Gap, mm	Width of the Gap, mm
20	250	85	750	3	720

The following assumptions were used when conducting the FSI study:

- The polymer melt is a incompressible non-Newtonian fluid;
- The polymer flow is assumed to be isothermal, laminar, and fully developed;
- There is a no-slip condition between die wall and polymer melt.

The boundary conditions for the solid and fluid domains were defined based on the schematics shown in Figure 3.

For the solid part, there are two symmetrical planes and solid–fluid interface as shown in Figure 3a. Ansys Static–Structural was used for the computation of the die body deformation. It is assumed that the upper symmetry of the solid domain is fixed, as in reality this face of the die is bolted. The FSI coupling data exchange between the fluid flow and solid structure appears at the solid–fluid interface.

The fluid domain was simulated using Ansys Fluent. At the inlet, the flow is assumed to be fully developed with the certain mass flow rate. For the die wall, the no-slip boundary condition was applied. This implies zero normal and tangential velocities at the wall. Along the symmetrical planes, zero normal velocities and zero shear rates are applied. The outlet boundary conditions were defined as zero normal and tangential forces (Figure 3b).

4. Discussion

In this section, the performance of the coat-hanger die geometry obtained was evaluated with regard to different operating flow rates and different extrusion materials. Overall, five FSI simulations were conducted using the system coupling component in Ansys Workbench 15.9, which allows data exchange between Ansys Fluent and Ansys Structural. First, three simulations were performed on the flow of material #1 with three different mass flow rate values ($\dot{m}_1$, $\dot{m}_2$, $\dot{m}_3$). The last two simulations were performed on material #2 and #3 with the mass flow rate $\dot{m}_1$. Table 2 contains the summary of all simulations based on the material used and the mass flow rate value. The rheological properties of the extrusion materials are provided in Table 3.

Table 2. Summary of simulations.

Simulation #	Mass Flow Rate	Material
1	$\dot{m}_1 = 0.011488$ kg/s	Material #1
2	$\dot{m}_2 = 0.055555$ kg/s	Material #1
3	$\dot{m}_3 = 0.069444$ kg/s	Material #1
4	$\dot{m}_1 = 0.011488$ kg/s	Material #2
5	$\dot{m}_1 = 0.011488$ kg/s	Material #3

Table 3. Extrusion materials.

Material #	Rheological Properties
Material #1	Casson model: $\tau_0 = 1.062$ Pa, k = 0.0271 Pa·s, n = 0.4127 [21]
Material #2	Carreau–Yasuda model: $\eta_{ref} = 16,968$ Pa s, $\lambda_{ref} = 1.224$, n = 0.4127, a = 1 [5]
Material #3	Power-law model: K = 26,500 Pa·s, n = 0.22 [4]

Figure 4 represents how the outlet velocity of the given coat-hanger die varies with changing mass flow rate but using the same material. In turn, Figure 5 represents the outlet flow rate variation with regard to material change.

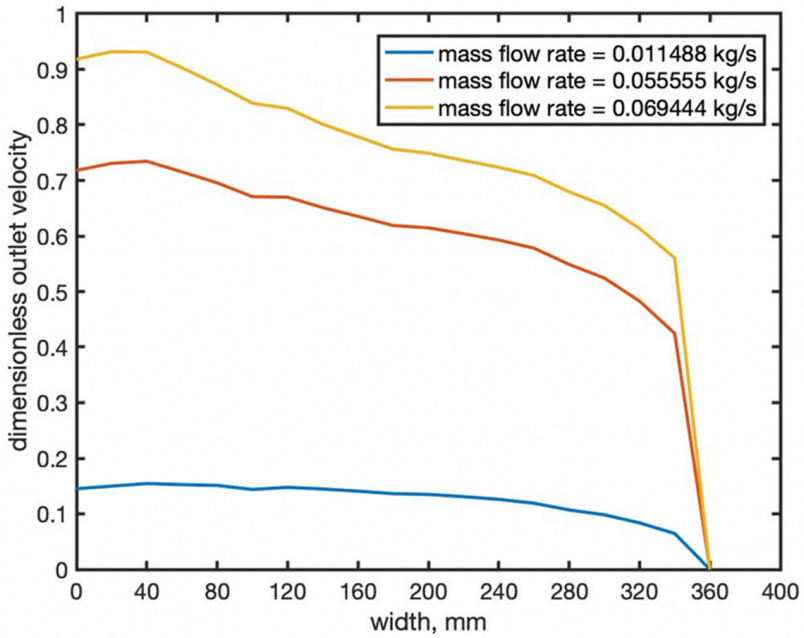

Figure 4. Outlet velocity distribution with changing mass flow rate.

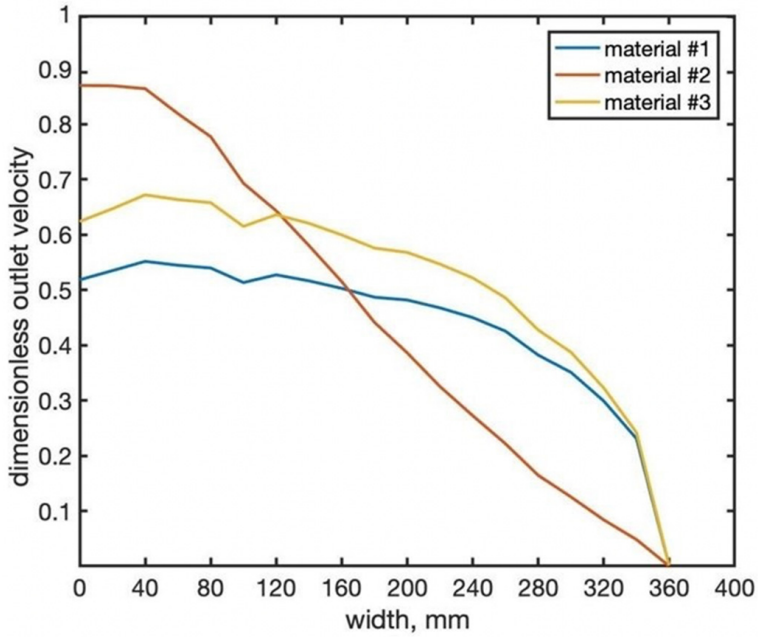

Figure 5. Outlet velocity distribution for three different extrusion materials.

According to Figure 4, the homogeneity of outlet velocity is not significantly affected by increasing the flow rate value. However, the stagnation zone where the manifold and slit regions intersect at the center becomes noticeable with increasing mass flow rate (Figure 6). In practice, the stagnation zones result in hold-up or degradation [6].

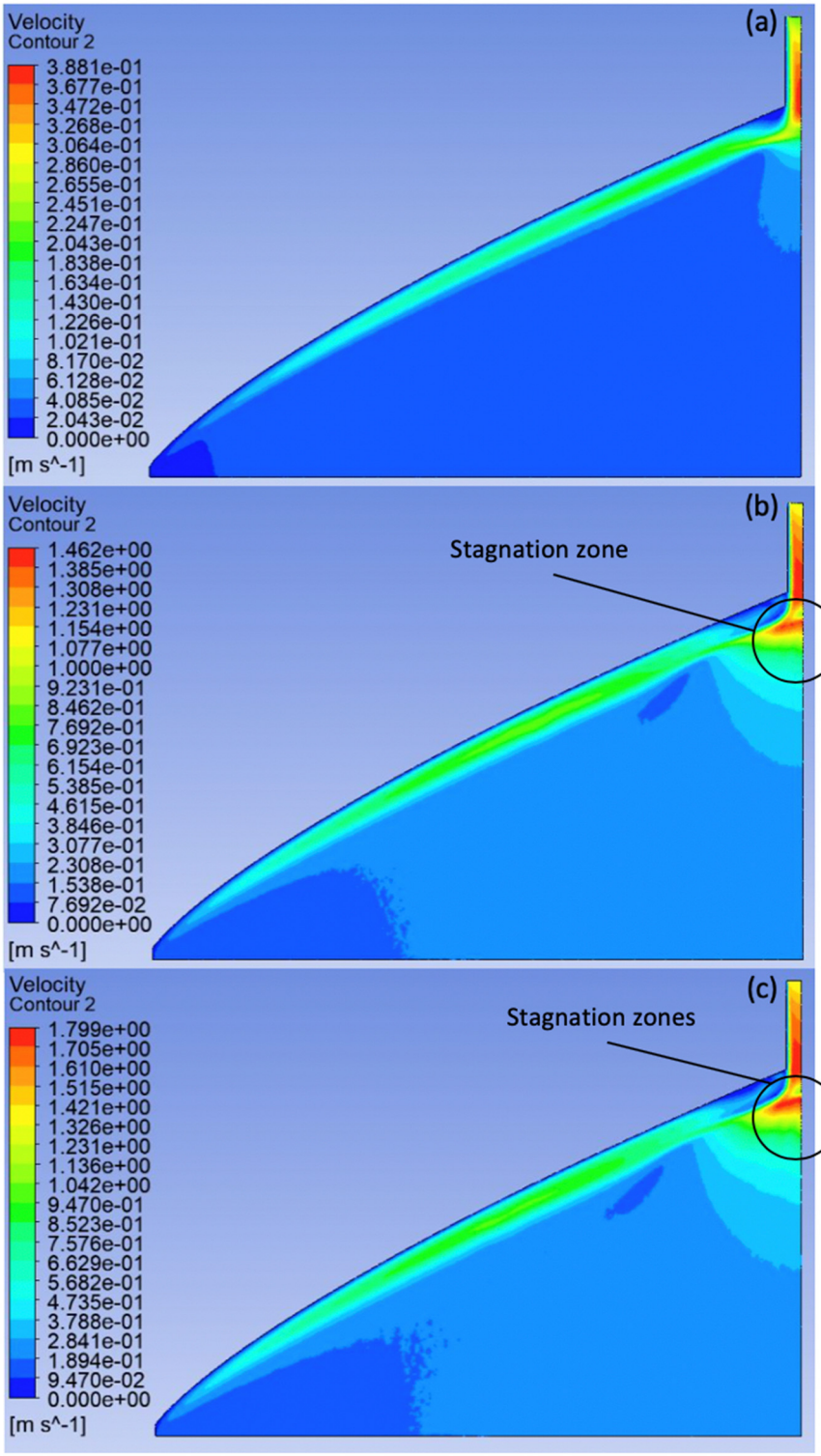

Figure 6. Velocity contour plots of extrusion material #1 with (**a**) $\dot{m}_1 = 0.011488\,\mathrm{kg/s}$, (**b**) $\dot{m}_2 = 0.055555\,\mathrm{kg/s}$, and (**c**) $\dot{m}_3 = 0.069444\,\mathrm{kg/s}$.

It can also be noticed from Figure 5 that this design cannot be used for the extrusion of material #2. The velocity sharply decreases as it goes from the center to the edge. In practice, the outlet flow variation of the coat-hanger dies should not exceed 5% [5]. For material #2, the manual adjustment of the manifold edge to reduce the outlet flow variation will be time-consuming. In turn, for materials #1

and #3 the outlet velocity is comparatively uniform. However, for extrusion material #2 and #3 there are no stagnation zones as shown in Figure 7.

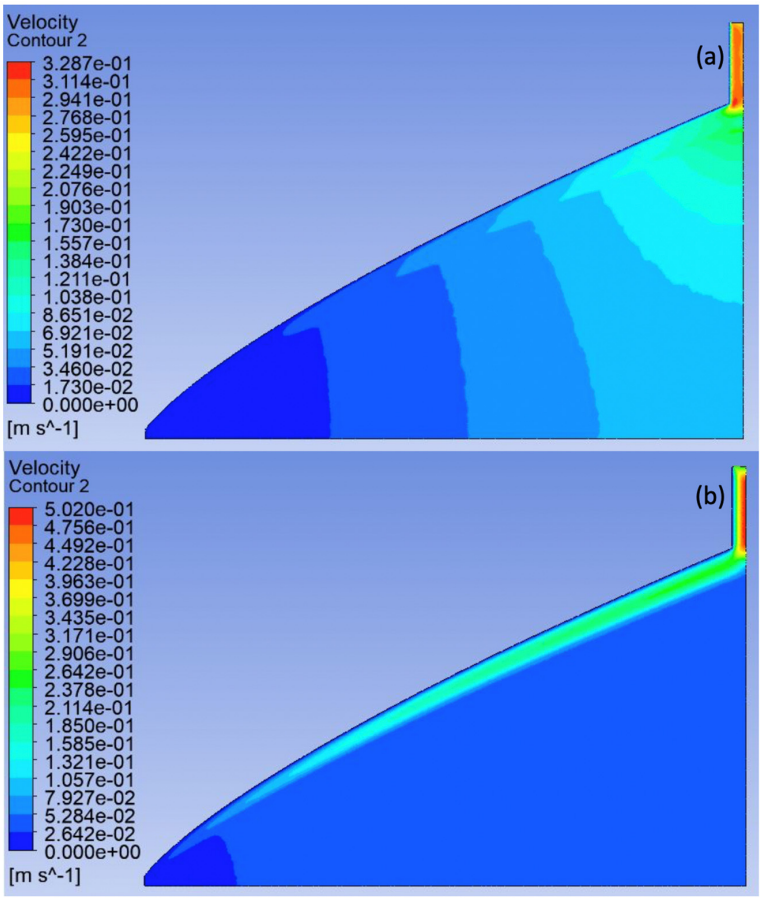

Figure 7. Velocity contour plots of extrusion: (**a**) material #2 and (**b**) material #3.

Table 4 represents the die exit average velocity variation in percentage for all FSI simulations. The extrusion of material #2 results in the highest value of outlet velocity variation.

Table 4. Die exit average velocity variation.

Simulation #	#1	#2	#3	#4	#5
Die exit average velocity variation	15.2%	10.9%	11.6%	52.5%	17.9%

From the above, it can be concluded that the outlet velocity of the geometry created is sensitive to the material type. In addition, defining the appropriate range of the mass flow rate values to prevent the formation of stagnation zones is recommended. Despite that the simulations #2 and #3 with increased mass flow rates perform better in terms of outlet velocity variation, the presence of stagnation zones may cause production problems.

In this FSI study, it was determined that the deformation of the solid die body is also sensitive to the material type rather than the increasing flow rate. According to Figure 8, the maximum deformation values occurring at the center of the outlet for $\dot{m}_1 = 0.011488$ kg/s, $\dot{m}_2 = 0.055555$ kg/s, and $\dot{m}_3 = 0.06944$ kg/s are $8.4{\cdot}10^{-10}$, $4.0{\cdot}10^{-9}$, and $5.1{\cdot}10^{-9}$ m, respectively. In addition, the following deformation values (Figure 9) are obtained when simulating the flow of material #2 and #3 with the $\dot{m}_1 = 0.011488$ kg/s: $3.9{\cdot}10^{-5}$ m and $8.9{\cdot}10^{-4}$ m, respectively. Table 5 provides the ratios of the

deformation value to the thickness of polymer at the exit and values of the von Mises stress to ensure that the die body remains elastic. To sum up, material #1 with the three different flow rate values causes much less deformation in comparison with material #2 and #3 with the flow rate of $\dot{m}_1 = 0.011488$ kg/s. According to Table 5, the maximum von Mises stress value for material #3 exceeds the yield strength of the die material at some locations. However, this small region with high stress elements is located in the manifold channel, which cannot be subjected to the displacement at this stress value (Figure 10). These high stress points can be avoided by reducing the operating flow rate.

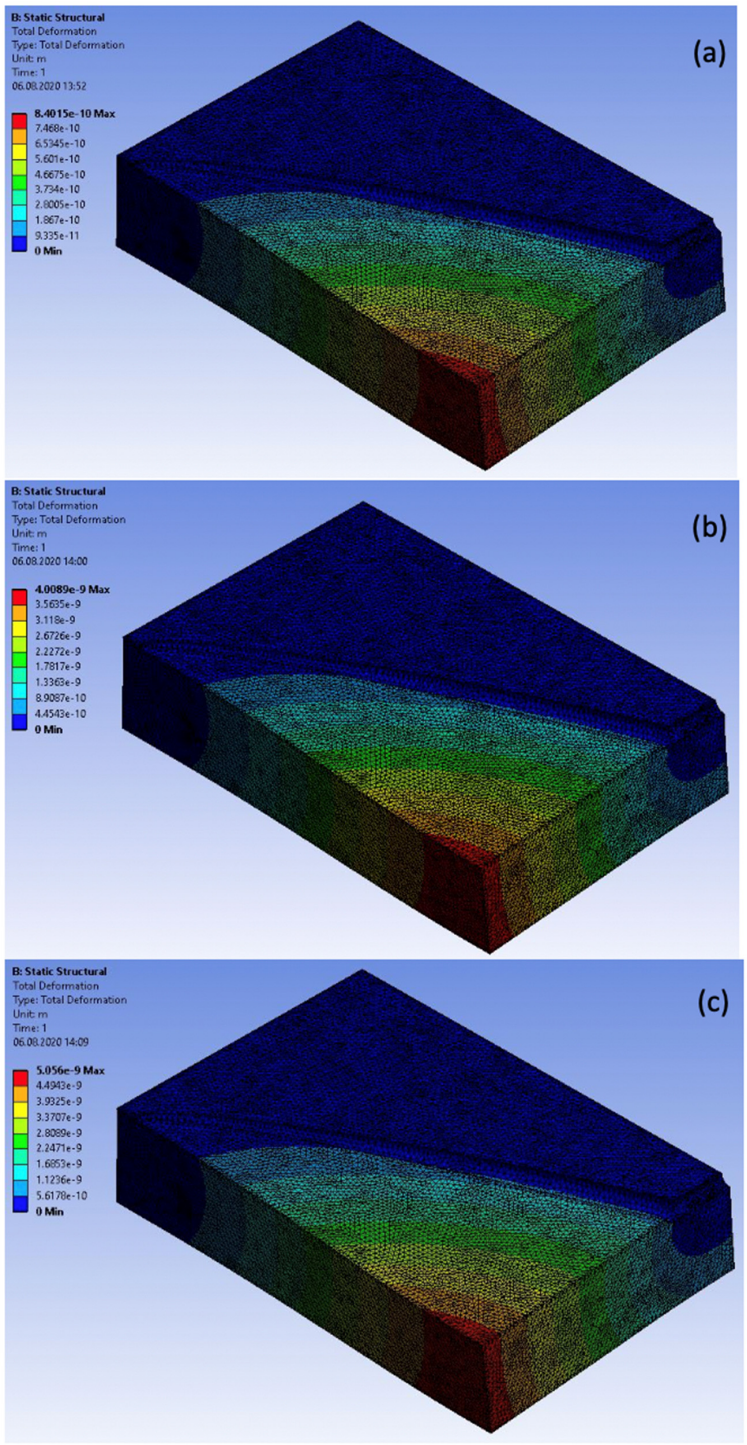

Figure 8. Deformation contour plots of extrusion material #1 with (**a**) $\dot{m}_1 = 0.011488$ kg/s, (**b**) $\dot{m}_2 = 0.055555$ kg/s, and (**c**) $\dot{m}_3 = 0.069444$ kg/s.

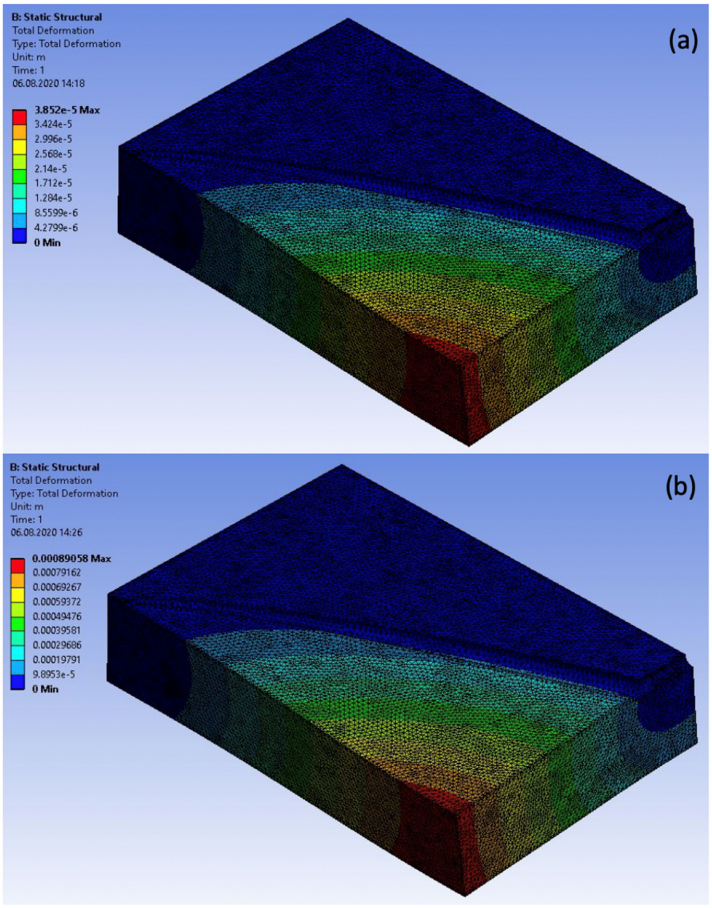

Figure 9. Deformation contour plots of extrusion: (**a**) material #2 and (**b**) material #3.

Table 5. Ratio of the maximum deformation value to the thickness of the solid die body.

Simulation #	#1	#2	#3	#4	#5
$\frac{\text{Deformation}}{\text{Polymer thickness at the exit}}$	$2.8{\cdot}10^{-7}$	$1.3{\cdot}10^{-6}$	$1.6{\cdot}10^{-6}$	$1.3{\cdot}10^{-2}$	$2.9{\cdot}10^{-1}$
Maximum von Mises stress, Pa	2020.5	9563.9	12040	$9.5{\cdot}10^{7}$	$1.1{\cdot}10^{9}$

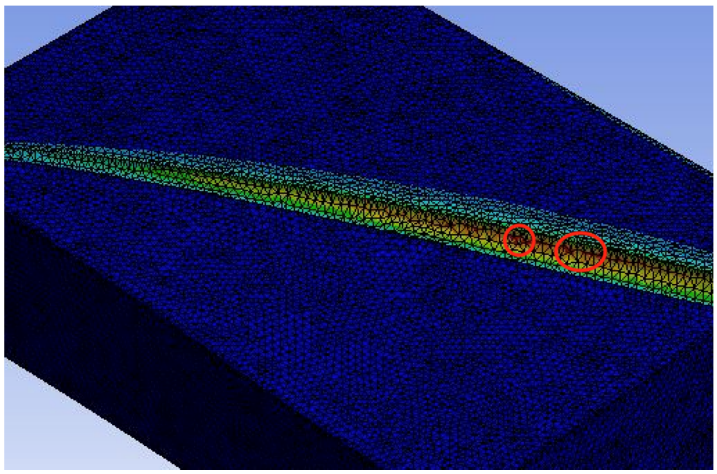

Figure 10. High stress elements: material #3.

This FSI study also determined the pressure distribution for the coat-hanger die design obtained. Overall, for the uniformity of the flow, the pressure contour lines should be parallel to the die outlet.

According to Figures 11 and 12, the contour lines become oblique at the edge of the die for all three materials being extruded. Contour lines can also be improved by manually adjusting the edge of the die geometry. The extrusion of material #1 represents the lowest pressure values across the die because it has very low viscosity compared to material #2 and #3.

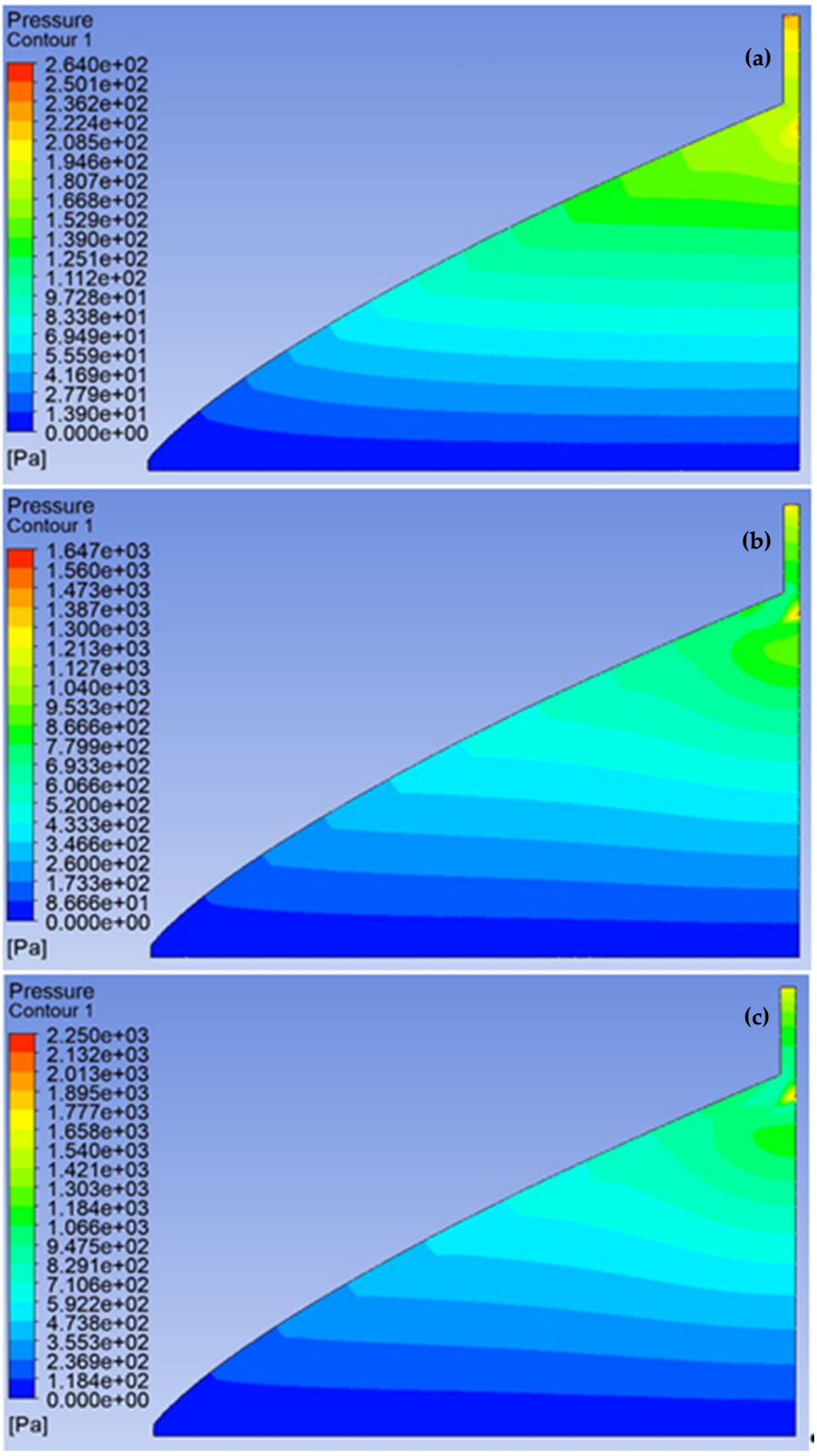

Figure 11. Pressure contour plots of extrusion material #1 with: (**a**) $\dot{m}_1 = 0.011488\,\mathrm{kg/s}$, (**b**) $\dot{m}_2 = 0.055555\,\mathrm{kg/s}$, and (**c**) $\dot{m}_3 = 0.069444\,\mathrm{kg/s}$.

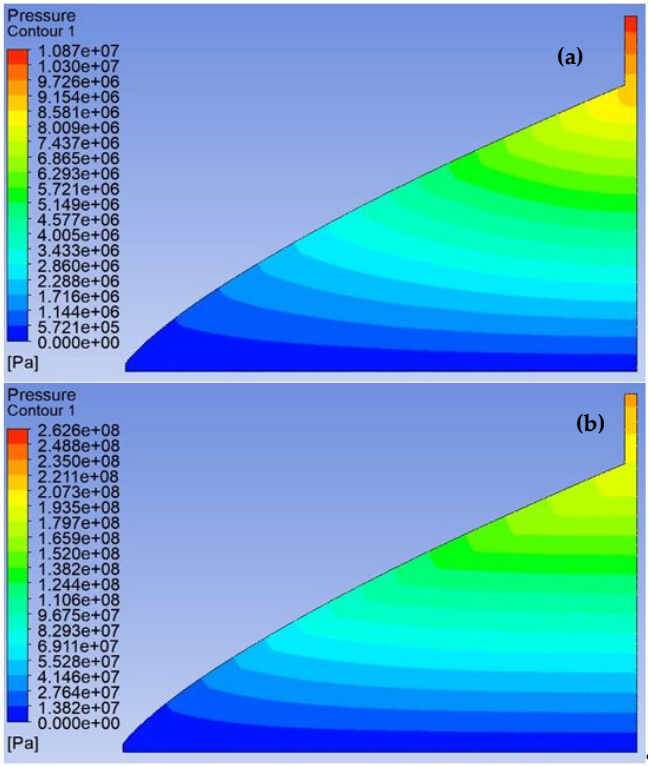

Figure 12. Pressure contour plots of extrusion: (**a**) material #2 and (**b**) material #3.

5. Conclusions

The methodology to derive the design equations of the uniform shear rate coat-hanger based on the Casson viscosity model was developed. This procedure can be applied for the design of the coat-hanger die depending on the product size, material being extruded, and operating mass flow rate required. The FSI study was conducted to assess the homogeneity of the outlet velocity and deflection of the solid die body. It was concluded that the geometry obtained can only be used for the extrusion of initial material (with $k = 0.0271$ Pa·s and $n = 0.4127$) for which it was designed. In addition, despite the fact that the homogeneity of the outlet velocity was not significantly affected by the increasing mass flow rate, the specific range of the allowed mass flow rate should be calculated to prevent the stagnation. The FSI study also determined that the deformation value of the solid die body is sensitive to the material change rather than the flow rate increase.

Overall, the methodology proposed for the mathematical modeling of the coat-hanger die is the acceptable approach for the initial design. However, further manual adjustments are required to improve the flow uniformity at the manifold edge for material #1. For the extrusion of material #2, the manifold adjustment will be time-consuming, while for material #3 the operating flow rate of the machine should be reduced.

Author Contributions: D.W., A.P., and D.Z. conceived the idea of this research; D.I. and A.P. developed the framework of the paper; D.W. provided the key ideas for solving Equation (42), leading to the design Equations (47) and (53); D.I. developed the design equations and carried out numerical simulations; A.P. and D.Z. performed the detailed analysis of the structural part of the FSI study; D.I. prepared the manuscript under the supervision of A.P., D.W., and D.Z. All authors have read and agreed to the published version of the manuscript.

Funding: This research and APC was funded by Ministry of Education and Science of the Republic of Kazakhstan under grant number. AP05134166.

Acknowledgments: This research was funded under the target program No. AP05134166 "Development and Prototyping of Extrusion Dies for Advanced Plastic Sheets and Thin Film Production" from the Ministry of Education and Science of the Republic of Kazakhstan. The authors would like to acknowledge the support received from the Ministry of Education and Science of the Republic of Kazakhstan and School of Sciences and Humanities, Nazarbayev University.

Conflicts of Interest: The authors declare no conflict of interest.

References

1. Wu, T.; Jiang, B.; Xu, S.; Huang, N. Three-dimensional nonisothermal simulation of a coat hanger die. *J. Appl. Polym. Sci.* **2006**, *101*, 2911–2918. [CrossRef]
2. Matsubara, Y. Geometry design of a coat-hanger die with uniform flow rate and residence time across the die width. *Polym. Eng. Sci.* **1979**, *19*, 169–172. [CrossRef]
3. Chung, C.I. Die Designs. In *Extrusion of Polymers: Theory & Practice*, 2nd ed.; Hanser Verlag: Munich, Germany, 2019; pp. 373–412.
4. Kopplmayr, T.; Aigner, M.; Miethlinger, J. A Comparative Study of Viscous Flow in Slit-Exit Cross Section Dies Using Network Analysis. *J. Plast. Technol.* **2012**, *8*, 54–73.
5. Vlachopoulos, J.; Polychronopoulos, N.; Tanifuji, S.; Müller, J.P. Flat Film and Sheet Dies. In *Design of Extrusion Forming Tools*, 1st ed.; Carneiro, O., Nobrega, J.M., Eds.; Smithers Rapra: London, UK, 2012; pp. 113–140.
6. Huang, Y.; Gentle, C.R.; Hull, J.B. A comprehensive 3-D analysis of polymer melt flow in slit extrusion dies. *Adv. Polym. Technol.* **2004**, *23*, 111–124. [CrossRef]
7. Meng, K.; Wang, X.; Chen, Q. Fluid flow in coat-hanger die of melt blowing process: Comparison of numerical simulations and experimental measurements. *Text. Res. J.* **2011**, *81*, 1686–1693. [CrossRef]
8. Lee, P.C.; Dietsche, L.; Dooley, J.; Parashar, S. Improving Film Die Flow Uniformity Using Optimization Methods Coupled with Finite Element Computational Fluid Dynamics (CFD) Analysis. *Int. Polym. Process.* **2015**, *30*, 51–62. [CrossRef]
9. Smith, D.E.; Wang, Q. Optimization-based design of polymer sheeting dies using generalized Newtonian fluid models. *Polym. Eng. Sci.* **2005**, *45*, 953–965. [CrossRef]
10. Wang, Q.; Smith, D.E. Analysis of the fluid–structure interaction in the optimization-based design of polymer sheeting dies. *J. Appl. Polym. Sci.* **2006**, *103*, 3994–4004. [CrossRef]
11. Winter, H.H.; Fritz, H.G. Design of dies for the extrusion of sheets and annular parisons: The distribution problem. *Polym. Eng. Sci.* **1986**, *26*, 543–553. [CrossRef]
12. Casson, N. A Flow Equation for Pigment-Oil Suspensions of the Printing Ink Type. In *Rheology of Disperse Systems*; Mill, C.C., Ed.; Pergamon: New York, NY, USA, 1959.
13. Mukhopadhyay, S. Casson fluid flow and heat transfer over a nonlinearly stretching surface. *Chin. Phys. B* **2013**, *22*, 074701. [CrossRef]
14. Khan, M.I.; Waqas, M.; Hayat, T.; Alsaedi, A. A comparative study of Casson fluid with homogeneous-heterogeneous reactions. *J. Colloid Interface Sci.* **2017**, *498*, 85–90. [CrossRef] [PubMed]
15. Michaelides, E.E.; Crowe, C.T.; Schwarzkopf, J.D. Fluid–Solid Flow in Ducts. In *Multiphase Flow Handbook*; Informa UK Limited: London, UK, 2016; pp. 357–454.
16. Nandy, S.K. Analytical Solution of MHD Stagnation-Point Flow and Heat Transfer of Casson Fluid over a Stretching Sheet with Partial Slip. *ISRN Thermodyn.* **2013**, *2013*, 1–9. [CrossRef]
17. Ullah, I.; Alkanhal, T.A.; Shafie, S.; Nisar, K.S.; Khan, I.; Makinde, O.D. MHD Slip Flow of Casson Fluid along a Nonlinear Permeable Stretching Cylinder Saturated in a Porous Medium with Chemical Reaction, Viscous Dissipation, and Heat Generation/Absorption. *Symmetry* **2019**, *11*, 531. [CrossRef]
18. Lungu, M.; Petrovan, S.; Rusu, M.; Apetroaiei, A.; Lungu, A. Application of rheological models for the description of the flow characteristics of some polymer systems. *Acta Polym.* **1992**, *43*, 214–218. [CrossRef]
19. Matveenko, V.N.; Kirsanov, E.A. Structural Viscosity and Structural Elasticity of Polymer Melts. *Russ. J. Appl. Chem.* **2018**, *91*, 839–865. [CrossRef]
20. Hopmann, C.; Michaeli, W. Fundamental Equations for Simple Flows. In *Extrusion Dies for Plastics and Rubber: Design and Engineering Computations*, 4th ed.; Hanser Publications: Munich, Germany, 2016; pp. 49–82.
21. Gurauskis, J.; Baudín, C.; Sanchez-Herencia, A. Tape casting of Y-TZP with low binder content. *Ceram. Int.* **2007**, *33*, 1099–1103. [CrossRef]